ADVANCED SUSTAINABLE SYSTEMS
www.advsustainsys.com

Fluorescent Chitosan Hydrogels Based on Biomass-Derived Carbon Dots for Toxic Aromatic Detection

Imane Haddadou, Patrick Brisebois, Claudiane M. Ouellet-Plamondon, Daniele Benetti, and Federico Rosei*

This study presents a sustainable method for synthesizing anionic carbon dots (CDs) from food waste, specifically almond peels (AP) and butternut peels (BP) and seeds (BS), using a microwave-ultrasound process. The novelty of this work lies in the systematic investigation of thermal pretreatment (torrefaction) and its influence on the photoluminescence (PL) properties of biomass-derived CDs. Torrefaction enhances PL intensity in CDs synthesized from almond peels and butternut seeds, while having a limited effect on those from butternut peels. The resulting CDs exhibit excitation-dependent, blue-emitting fluorescence and maintain over 85% PL stability across the environmentally relevant pH range of 5–9. To enable pollutant detection, the optimized CDs are embedded into chitosan-based hydrogels, forming water-stable, reusable fluorescent sensors. These composites detect aromatic contaminants, including pentachlorophenol (PCP) and 4-chloro-2-methylphenoxyacetic acid (MCPA), with detection limits of 1.45 ± 0.08 and 4.10 ± 0.10 nM, respectively. The combination of waste valorization, surface-state modulation, and soft-material integration supports the development of cost-effective, environmentally friendly sensors. This initiave contributes to Sustainable Development Goals focused on clean water and responsible consumption by transforming food waste into functional materials for environmental monitoring.

1. Introduction

Chlorophenols (CPs) and phenoxy-acetic acids are persistent environmental contaminants originating from industrial and agricultural activities.[1] Pentachlorophenol (PCP) is a carcinogenic heavy-duty wood preservative, while 4-chloro-2-methylphenoxyacetic acid (MCPA) is a widely employed herbicide for broadleaf weed control.[2,3] Despite regulatory restrictions in various countries, both compounds continue to pose environmental threats due to their high mobility, chemical stability, and persistence in aquatic systems.[4,5] Consequently, strict limits have been established by global agencies, including the European Union (EU) (0.5 μg L^{-1} for PCP) and the World Health Organization (WHO) (2 μg L^{-1} for MCPA).[4,6]

Conventional analytical methods for detecting CPs, such as solid-phase extraction coupled with gas chromatography, though highly sensitive, are constrained by labor demands, lengthy protocols, and the need for advanced instrumentation.[7–9] These limitations drive the demand for more accessible, rapid, and cost-effective alternatives. Fluorescent sensing offers a compelling solution, enabling real-time, sensitive detection with minimal operational complexity.[10,11] These sensors can function as solution-based probes,[12] or be embedded into solid materials for enhanced robustness and practical deployment.[13]

I. Haddadou, P. Brisebois, C. M. Ouellet-Plamondon
École de technologie supérieure
Université du Québec
1100 Notre-Dame Ouest, Montréal, Québec H3C 1K3, Canada
E-mail: Claudiane.Ouellet-Plamondon@etsmtl.ca

D. Benetti, F. Rosei
INRS
1650 Boulevard Lionel-Boulet, Varennes, QC J3×1P7, Canada

D. Benetti
Department of Chemistry
McGill University
801 Sherbrooke Street West, Montreal, QC H3A 0B8, Canada

D. Benetti
Department of Chemistry, Imperial College London
82 Wood Ln, London W12 0BZ, UK

F. Rosei
Department of Chemical and Pharmaceutical Sciences
University of Trieste
Via Giorgeri 1, Trieste 34127, Italy

The ORCID identification number(s) for the author(s) of this article can be found under https://doi.org/10.1002/adsu.202500689

DOI: 10.1002/adsu.202500689

Fluorescent hydrogels have emerged as multifunctional platforms for sensing, drug delivery, tissue engineering, and optoelectronic applications.[14–16] They naturally respond to changes in pH, temperature, or specific molecules, enabling real-time, sensitive analyte detection.[17] These soft, 3D networks are typically formed from natural or synthetic polymers tagged with fluorophores.[18] Among them, chitosan (CH) stands out as a versatile, biocompatible polysaccharide, readily assembled via physical or chemical cross-linking to yield stable hydrogel matrices.[19,20]

Carbon dots (CDs) have recently enabled multifunctional applications spanning chemical sensing,[21–23] biological detection,[24,25] bioimaging,[26,27] drug delivery,[28–30] and lighting technologies.[31–33] These fluorescent nanomaterials exhibit exceptional water solubility, low toxicity, and robust chemical stability.[34] CDs synthesis leverages diverse methods including chemical/electrochemical oxidation, pyrolysis, carbonization, and ultrasonic treatment.[35] The bottom-up approaches employing precursors ranging from simple organic molecules (e.g., urea, citric acid)[36] to complex biomass (e.g., lemon,[37] quince fruit,[38] and plant leaves[39]), polymers and waste derivatives (e.g., peels,[40] seeds,[41] and combustion residues[42]). Although protocols utilize raw[43] or following pretreatment,[44] the role of pretreatment in tuning their structural and optical properties remains largely neglected. Certain pretreatment techniques, such as carbonization and torrefaction, can significantly improve both material quality and CDs yield,[45] yet remain underexplored in this context.

In this study, we present a sustainable and scalable strategy for synthesizing anionic CDs via a hybrid microwave–ultrasound method using three underutilized food wastes as carbon sources, specifically almond peels (*Prunus dulcis*) (AP), butternut peels (BP) and seeds (BS) (*Cucurbita moschata*). We systematically investigate how thermal pretreatment (torrefaction) of biomass modulates the fluorescence and stability of the resulting CDs, an aspect that remains largely overlooked in the literature. While prior research has utilized raw or processed biomass for CD synthesis, the systematic correlation between thermal pretreatment conditions and pH-dependent fluorescence amplification remains largely unaddressed.

The optimized CDs are embedded into chitosan-based hydrogel matrices, yielding reusable, water-stable fluorescent sensors. These composite materials enable rapid, ultrasensitive detection of aromatic water pollutants (PCP and MCPA) through tunable fluorescence quenching. This dual-component system integrates the tunable fluorescence of CDs with the molecular affinity of chitosan, enabling high sensitivity and operational simplicity for real-time pollutant detection in aqueous environments.

Our findings significantly advance the understanding of how biomass pretreatment strategies influence CD properties, paving the way for more deliberate design of waste-derived nanomaterials. Beyond its analytical performance, this work represents a green chemistry approach that valorizes renewable kitchen waste into functional materials for environmental applications. By correlating feedstock modification with sensing performance, we establish a scalable framework for the development of low-cost, high-efficiency sensors.

This contribution directly supports the United Nations Sustainable Development Goals (SDGs)—specifically, clean water and sanitation and responsible consumption and production—by demonstrating how food waste can be transformed into high-value, eco-friendly sensing platforms. Our approach merges resource recovery with environmental monitoring, offering a practical solution to pressing global challenges in pollution control and sustainable material development.

2. Experimental Section and Methodology

2.1. Experimental Section

2.1.1. Materials

All chemicals were used as received and without purification. +37.0% ACS grade hydrochloric acid and +99.0% sodium hydroxide were purchased from Anachemia (Qc, Canada). Water was purified using a Direct-Q 8UV Millipore system.

2.1.2. Synthesis of CDs

As presented in **Figure 1**, a mixture of grounded carbon precursors and water (1:100, w/w) was heated to 220 °C in a microwave reactor and maintained at this temperature for 30 min. The resulting brown suspension was sonicated for 5 min and then centrifuged at 13 000 rpm for 60 min. The supernatant was filtered through a 0.20 µm syringe filter and dialyzed against deionized water through a dialysis bag (Molecular weight cut-off = 0.5–1 kDa) for 24 h to remove any unreacted molecules. Finally, a light brown CD powder was collected by lyophilization and stored in the dark at 4 °C for further characterization and use.

2.1.3. Hydrogel Preparation

Various proportions of differentCDs were dispersed in 0.1 M acetic acid (6 mL), and the obtained solutions were mixed with glycerol (4 mL). 0.1 g of chitosan was subsequently dissolved in the previous mixture and mechanically stirred until a completely transparent solution was obtained. Under continuous stirring, 0.3 mL of 5N NaOH solution was added drop by drop to neutralize the chitosan solution. The formed gel was repeatedly washed to remove all unreacted chitosan residues, then filtered, cast onto petri plates, and dried at 60 °C. Finally, the dried gel was slightly wetted with water and kept in a vacuum at room temperature. The chitosan hydrogel samples were coded as CH_0, $CH_{0.25}$, $CH_{0.5}$, and CH_1 according to the CDs weight proportions in the hydrogel, including 0, 0.25, 0.5, and 1 wt%, respectively (based on the final hydrogel weight).

2.1.4. Fluorescence Activity

To measure the sensitivity of the as-prepared hydrogel CH_1 to PCP and MCPA, a set of 13 solutions with different concentration levels of each pollutant 0.0001, 0.0005, 0.001, 0.005, 0.01, 0.05, 0.1, 0.5, 1, 5, 10, 50 and 100 µM) was prepared and a small section of hydrogel (≈1 × 1 cm^2) was immersed in 5 mL of each

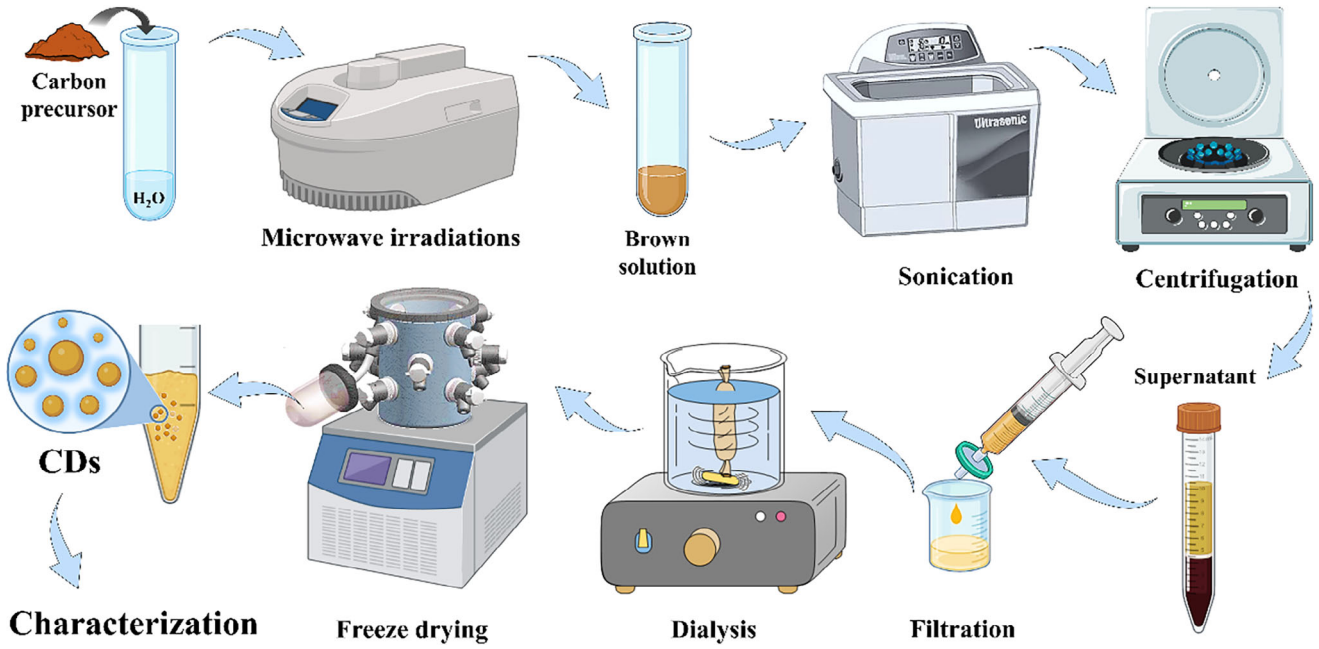

Figure 1. The schematic synthesis process of CDs.

solution, at room temperature. After 2 h, the hydrogels were collected from the pollutant solutions, and their fluorescence spectrum was recorded at an excitation wavelength of 340 nm. The variation in fluorescence $(F_0\text{-}F)/F_0$ was then plotted against each concentration of the pollutant solution, where F_0 and F are the fluorescence intensity of the hydrogel in the presence and absence of these two aromatic polluants, respectively. The limit of detection (LOD) and the limit of quantification (LOQ) were calculated following Equations (1) and (2) below, respectively, where: SD_{blank} is the standard deviation of the 10-blank measurement, I_{blank} and I_{sample} are the mean fluorescence intensities for the blank and sample, respectively, and C is the concentration of the analyte in the solution.

$$LOD = \frac{3 \times SD_{blank}}{(I_{sample} - I_{blank})} \times C \quad (1)$$

$$LOQ = \frac{10 \times SD_{blank}}{(I_{sample} - I_{blank})} \times C \quad (2)$$

To evaluate the reusability of the hydrogel after the detection experiments, the samples collected from the first sensing were rinsed thoroughly with deionized water and subsequently reused under the same conditions.

3. Methods

3.1. Microwave Synthesizer

The microwave-assisted synthesis of CDs was performed using a CEM Discover SP Microwave Synthesizer at 300 W. Typically, a heating ramp of 20 °C/min was applied for 10 min, then the solution was heated at 220 °C for 30 min. Finally, the solution was cooled to r.t. at a rate of 10 °C °C/min for 20 min (Figure S1, Supporting Information).

3.2. Ultrasonic Treatment

The ultrasonic treatment was performed using an ultrasonic bath, Branson 5200 at r.t. for 5 min.

3.3. Zeta Potential Measurements

The surface charge was evaluated by analyzing a solution of 0.5 mg of CDs in 1 mL of deionized water (pH ≈7) at 25 °C using a Brookhaven Zeta Plus instrument.

3.4. UV-Visible Spectroscopy

The UV-Vis absorption emission spectra of the CDs in water were measured using a Cary 300 Bio (Varian) spectrophotometer. Zeroing using ultrapure water was applied systematically to eliminate the signals of water and the quartz cell in all experiments.

3.5. Fluorescence Spectroscopy

The fluorescence emission spectra of the CDs in water were measured using a Cary Eclipse (Varian) spectrofluorometer. Zeroing using ultrapure water was applied systematically to eliminate the signals of water and the quartz cell in all experiments.

3.6. Fourier Transform Infrared (FTIR) Spectroscopy

FTIR spectra were collected on a Spectrum Two FTIR spectrophotometer (Perkin-Elmer, Canada), and 10 scans were acquired in the spectral window between 400 to 4000 cm^{-1} with a resolution of 0.4 cm^{-1}. Background correction was applied automatically to eliminate the signals of atmospheric moisture and carbon dioxide.

3.7. X-ray photoelectron spectroscopy (XPS)

XPS measurements were carried out using a VG Escalab 220i-XL spectrometer equipped with a hemispherical analyzer and an Al K_α twin anode X-ray source (E = 1486.6 eV). The instrument was calibrated using the C1s peak at 284.8 eV.

3.8. Statistical Analysis

Data are presented as means ± SD of independent replicates (n = 3). Error bars represent SD. Two-way ANOVA with Tukey's post-hoc testing assessed main effects (biomass type, pretreatment) and their interactions across all experiments. Significance was defined at $\alpha = 0.05$ (two-tailed), with null hypotheses rejected when $p < \alpha$.

4. Results and Discussion

4.1. Preparation of CDs From Biomass

The biomass precursors used in this study, almond peels (AP), butternut peels (BP), and seeds (BS), were procured from local grocery sources, reflecting readily available and low-cost feedstocks suitable for scalable, sustainable applications. Prior to carbon dot (CD) synthesis, all biomass materials were air-dried, then ground into a fine powder to increase the surface area and improve the efficiency of subsequent thermal conversion (Figure S1, Supporting Information).[46]

Two experimental conditions were applied: untreated biomass and pretreated (P) biomass. The pretreatment step consisted of oxidative torrefaction at 220 °C for 1 h, a process known to decompose hemicellulose and partially depolymerize lignocellulosic structures.[47,48] This thermochemical modification enriches the biomass in carbonaceous content, reduces oxygen-containing groups, and promotes the generation of aromatic intermediates favorable for CD formation. The pretreated powders were stored in dry, sealed containers to prevent moisture uptake prior to synthesis.

The CDs were synthesized using a microwave-assisted hydrothermal process, followed by ultrasonication. In a typical synthesis, the biomass powder (pretreated or untreated) was dispersed in deionized water and subjected to microwave heating in a closed-vessel reactor (at 220 °C for 30 min) (Figure S2) 1. The selection of 220 °C for microwave synthesis was guided by robust prior optimization studies, which identified this temperature as optimal for maximizing carbonization efficiency in both brewery spent grain,[21] and quince fruit-derived carbon dots, achieving a balanced quantum yield of 8.55%.[38] In summary, 220 °C was chosen as the optimal compromise to maximize both carbonization yield and fluorescence performance. Microwave irradiation enables rapid and volumetric heating, accelerating dehydration, decarboxylation, and carbonization reactions while maintaining uniform temperature and pressure conditions throughout the reaction medium.[49,50]

The conversion of biomass to CDs under microwave irradiation is primarily driven by the thermal degradation of lignocellulosic components. Cellulose, hemicellulose, and lignin. These polymers undergo hydrolysis and depolymerization, forming smaller sugars, organic acids, and phenolic compounds. Dehydration and decarboxylation then produce key intermediates like furfural and aromatics. These intermediates undergo aromatization, nucleation, and carbonization to form graphitic or amorphous carbon cores with oxygen- and nitrogen-containing surface groups.[51] Microwave energy enhances dipole rotation and ionic conduction, accelerating bond cleavage and carbonization. The aqueous medium supports hydrothermal passivation, producing CDs with hydrophilic functional groups such as —OH and —COOH.[52,53] Torrefied biomass increases the concentration of reactive intermediates, leading to higher carbon yields and improved optical properties.

Post-synthesis, the resulting suspensions were centrifuged and filtered to remove large particulates. CDs were further purified by dialysis against deionized water for 48 h using a 1 kDa membrane, ensuring removal of small-molecule impurities while retaining nanostructures.[54,55] The purified CDs were then freeze-dried, yielding solid, brownish powders (**Figure 1**). For each biomass type (AP, BP, BS) and pretreatment condition, three (3) independent experimental series were conducted (Figure S3, Supporting Information). Each series was initiated with three (3) batches of 5 mg of biomass. Post-synthesis, the intermediate solutions from all three (3) batches were pooled, purified, and lyophilized to obtain consolidated CD products. The yield for each series (mass CD/mass biomass × 100) was calculated by combining the results of the three (3) batches, and the overall yield and standard deviation (mean ± SD) were calculated from the three (3) series. This approach minimizes inter-batch variability while enabling robust quantification of uncertainties (n = 3 yield values/group) and reflects real-world scalability where consolidated outputs are typical.

The synthesis yield of carbon dots was strongly influenced by both the biomass source and thermal pretreatment. ANOVA analysis ($p < 0.001$) confirmed a statistically significant enhancement, with pretreatment increasing yields by an average of 4.63% across all feedstocks (AP, BP, BS) (Table S1, Supporting Information). Final yields ranged from 18.5% to 30.0%, consistent with recent benchmarks in biomass-derived CDs synthesis, including yields of >42% from lignin/cellulose,[56] and 45.9% from acrylamide/chitosan.[57] Compared to earlier reports of sub-10% yields that limited scalability,[58] our results are on par with optimized two-step protocols (20–40%),[59] demonstrating that pretreatment effectively enhances production efficiency toward industrial feasibility.

This synthesis route not only offers improved reaction efficiency and product quality but also aligns with green chemistry principles by eliminating toxic solvents, minimizing reaction time, and valorizing biomass waste. The combined effect of

pretreatment and microwave-assisted synthesis offers a robust, scalable platform to produce high-performance CDs suitable for sensing applications.

4.2. Characterization of CDs

The chemical structure of the CDs and both pre-treated and untreated raw materials powder was investigated by FTIR (**Figure 2**). All samples exhibit similar FTIR spectra and band positions due to the similarity of the chemical compositions.

The FTIR spectra of raw materials have stretching vibration bands of phenolic/carboxyl O—H and N—H bonds at ≈3300 cm^{-1}, asymmetric and symmetric C—H bond at 2920 and 2850 cm^{-1}, carboxylic and amide C═O at ≈1740 cm^{-1}, aromatic C═C bond at 1620 cm^{-1}, aromatic C—O and phenolic O—H at ≈1230 cm^{-1}, C—O—C bond in cellulose and hemicellulose at ≈1160 cm^{-1} as well as aliphatic ether C—O and alcohol C—O stretching at ≈1030 cm^{-1}.[60] The peak at 1380 cm^{-1} was assigned to aliphatic CH_3 deformation.[23,61] After the pre-treatment, the intensity of peaks at ≈3300, ≈2920, ≈2850, ≈1735, and ≈1230 cm^{-1} decreased. This is probably due to the partial decomposition of weak structural components through a series of reactions (dehydration, decarboxylation, etc.) during the torrefaction of residues, resulting in a more hydrophobic surface.[62] Compared with pre-treated and untreated raw materials, the intensity of some characteristic peaks increases in the FTIR spectrum of the resulting CDs. The increase of the broadband at ≈3200 cm^{-1} assigned to O—H and N—H stretching vibrations is due to hydrolysis. The strong peaks at ≈1660, ≈1580, ≈1400, and ≈1080 cm^{-1} are attributed to the stretching vibration of carboxylic and amid C═O, C═C skeletal ring, aromatic C—N, and C—O/P—O bonds, respectively. Two small peaks assigned to C—O—C stretching vibration and aromatic C—H deformation were observed at ≈1290 and ≈875 cm^{-1}.[63–65] Unlike the other CDs samples, those prepared from BS presented a bending vibration of C—NH at 1450 cm^{-1} and its intensity is reduced by the torrefaction of the carbon source. The presence of amide (—CO—NH—) bonding is revealed by the peak shift from ≈1740 cm^{-1} (carboxyl C═O stretching) in the curve of original materials to ≈1660 cm^{-1} (amide C═O stretching) in the curve of CDs.[66] The intensity of this peak was higher in the CDs synthesized from the butternut seeds, as this carbon source contains more protein than the other raw materials. Other peaks at ≈1660, ≈1290, and ≈1080 cm^{-1} suggest that the surface of CDs contains oxygen-functional groups such as C═O, C—O, and O-H. All these surface moieties enhance the hydrophilicity and stability of the CDs in aqueous solutions.[67] Thus, according to FTIR analysis, oxygen-rich N-doped CDs have been successfully formed. These results are similar to those reported on CDs from lignocellulosic material.[68] Crucially, these structural modifications are expected to underpin the fluorescence enhancement in pretreated AP and BS-CDs through three interconnected mechanisms: (i) the conversion of isolated carboxyl groups (1740 cm^{-1}) to conjugated amide bonds (1660 cm^{-1}) creates intrinsic fluorophores with electron-donor-acceptor configurations,[23] (ii) the

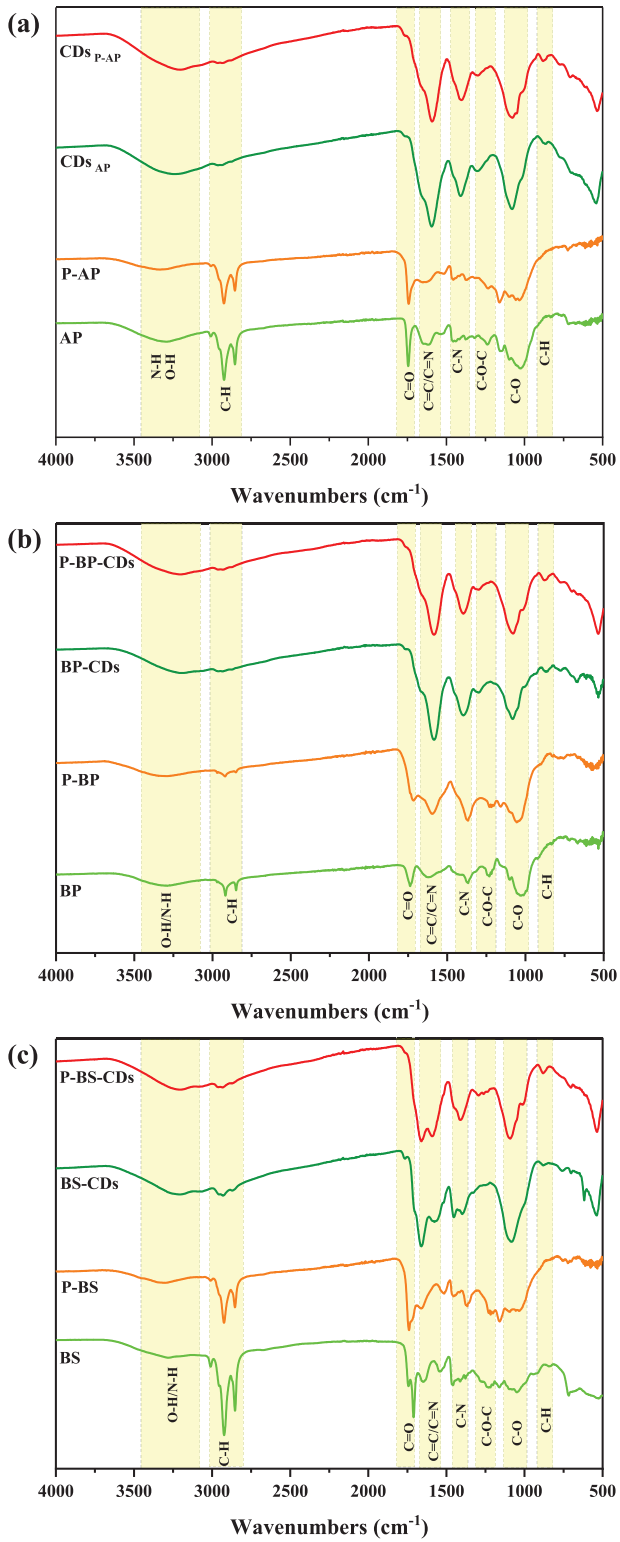

Figure 2. FTIR spectra of carbon dots prepared from a) almond peel (AP), b) butternut peel (BP), and c) butternut seeds (BS), with and without pretreatment (P).

reduction of aliphatic chains (diminished 2920/2850 cm^{-1}) coupled with intensified aromatic signatures (1580/1620 cm^{-1}) extends π-conjugation, lowering bandgap energy[69] and (iii) the enhanced hydrophilic functionalities (broadened 3200 cm^{-1}; intensified 1080 cm^{-1}) passivate surface defects through hydrogen bonding and hydration shell formation.[70] These synergistic effects amplify radiative recombination while suppressing non-radiative decay pathways. In contrast, BP-CDs show limited improvement due to persistent aliphatic character (1380 cm^{-1}), demonstrating biomass-specific torrefaction efficacy.

The XPS results provide insights into the elemental composition and surface chemistry of the prepared CDs, as detailed in the peak deconvolution of C1s, O1s, N1s, and P2p spectra, presented in Figures S4–S9 (Supporting Information). The CDs are primarily composed of carbon and oxygen, with an O:C atomic ratio ranging from 0.68 to 1.20 (Table S2, Supporting Information). Pretreatment increased the carbon content in CDs derived from BP but decreased in those from AP and BS. Oxygen content decreased across all samples, suggesting partial deoxygenation. This reduction is correlated with a decrease in carbonyl (C═O) and imine (C═N) groups, whereas hydroxyl (C—OH) and carboxyl (O—C═O) functionalities increased in CDs from pretreated AP and BS but decreased in BP-derived CDs. These findings align with FTIR-derived trends in oxygenated groups and zeta potential changes, supporting surface charge modifications.

Nitrogen doping ranged from 3.24% to 9.73%, with pyrrolic-N as the dominant species, followed by graphitic-N and pyridinic-N. After pretreatment, pyrrolic and graphitic N increased, while pyridinic N decreased, reflecting structural changes supported by FTIR spectral shifts. Phosphorus was also detected (0.34–1.18%), with an increase in phosphate-like (P—O) groups after pretreatment, particularly in CDs from AP, whereas BP- and BS-derived CDs contained more P—C groups.

Overall, XPS and FTIR results confirm that pretreatment improves the surface functionalities of CDs. It enhances hydrophilic and reactive groups, such as the hydroxyl, carboxylic, and ester groups, while increasing nitrogen content. Collectively, these chemical surface modifications are expected to enhance fluorescence through three electronic mechanisms: (i) Pyrrolic-N-induced mid-gap states (398.5 eV) provide radiative recombination centers, increasing quantum yield,[71] (ii) Carboxyl passivation (O—C═O at 288.1 eV) saturates non-radiative defect sites at graphitic edges,[72] and (iii) P—O/P—C modulation (133.4 eV) optimizes colloidal stability to prevent aggregation quenching.[73] In AP-CDs and BS-CDs, pretreatment synergizes these effects, narrowing band gaps while creating new emissive surface states.[74] Conversely, BP-CDs develop charge-trapping configurations due to P—C dominance and N-functionality loss, explaining their reduced PL.[75]

The optical properties of the carbon dots synthesized from biomass were characterized using UV-Visible spectroscopy.[76] All CDs showed similar UV–vis spectra with broad absorption bands in the UV region and extended tails to the visible region (**Figure 3**). Two shoulder peaks appeared ≈270 and ≈320 nm, corresponding to the $\pi \rightarrow \pi^*$ transition of aromatic C═C bonds and the $n \rightarrow \pi^*$ transition of the C═O moieties, respectively.[77] While the tail can be assigned to the transitions in the surface states of CDs.[78] These data are in agreement with previous studies on CDs obtained from other bio-sources such as fresh tomatoes,[79]

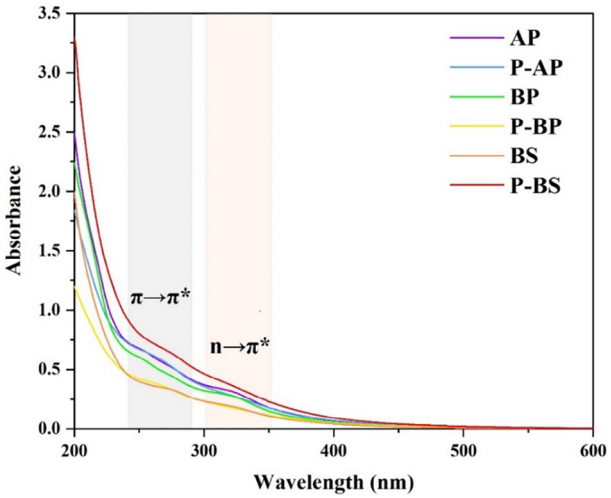

Figure 3. UV–vis absorbance spectra of carbon dots prepared from almond peel (AP), butternut peel (BP), and butternut seeds (BS), with and without pretreatment (P). (CDs concentration is 0.1 mg mL^{-1}).

roses,[80] cabbage,[81] or coriander.[82] This feature is indicative of the carbonaceous nature of the dots and suggests that the synthesis process effectively retains the conjugated structures that contribute to their optical properties.

Fluorescence emissions from as-prepared CDs were also investigated (**Figure 4**). As expected for most biomass-derived CDs, the different CDs show typical excitation-dependent fluorescence properties.[83] By increasing the excitation wavelength, the broad peaks observed at lower excitation energy become narrower and more symmetric. In addition, the peak position shifted first to lower wavelengths (blue shift), then to higher wavelengths (redshift). Photoluminescence (PL) emission intensity increases to reach a maximum before a progressive diminution. CDs from AP show a maximum emission centered at ≈432 nm when λ_{ex} = 350 nm, while BP and BS show a maximum emission centered at ≈423 and 422 nm when λ_{ex} = 340 nm. After pretreatment of PB, the PL emission of CDs presents an apparent redshift (15 nm), while this is not observed for CDs obtained from AP and BS from untreated samples.

Excitation at 340 nm (emission: 430 nm) revealed that pretreatment enhanced PL intensity for P-AP (≈1.16-fold) and P-BS (≈1.23-fold) CDs, but reduced it for BP (≈10%), showing precursor-dependent effects (Figure S10, Supporting Information). Two-way ANOVA confirmed significant effects of pretreatment ($p < 0.0001$) and biomass type ($p = 0.0002$), with a highly significant pretreatment × biomass interaction ($p<0.0001$). PL peaks red-shifted by 15 nm (BP), 8 nm (BS), and 3 nm (AP). Higher pyrrolic-N, confirmed by XPS, likely increased fluorescence efficiency and contributed to the excitation-dependent PL of the CDs.

Preliminary observations indicate that the CDs synthesized from pretreated biomass exhibit enhanced fluorescence intensity compared to their untreated counterparts. This enhancement can be attributed to the increased carbon content and reduced oxygen functional groups resulting from the torrefaction process. The torrefaction process not only facilitates the formation of more graphitic structures but also suppresses non-radiative

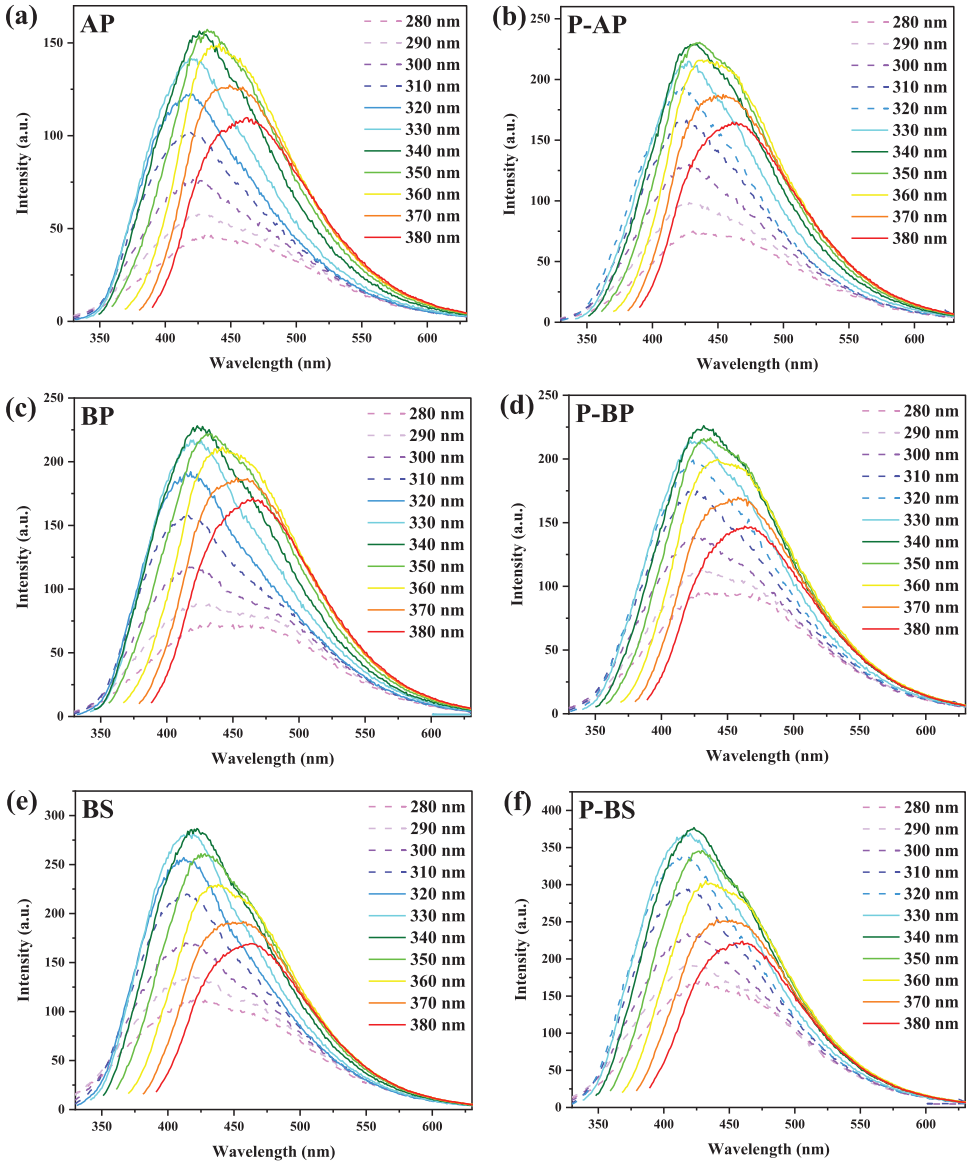

Figure 4. Excitation-dependent fluorescence emission spectra of carbon dots prepared from almond peel (AP), butternut peel (BP), and butternut seeds (BS), with and without pretreatment (P) at different excitation wavelengths (CDs concentration is 0.5 mg mL^{-1}). The dashed spectra correspond to the blue-shift effect, and the solid ones are used to label the red shift.

decay pathways, thereby promoting efficient light emission.[84,85] The suppression of vibrational modes in the fluorescent centers during the carbonization process leads to improved photoluminescence, a phenomenon known as supramolecular cross-linking-enhanced emission.[84]

The surface charge of CDs plays a crucial role in determining their stability, dispersibility, and interaction with fluids and hydrogels.[86] At neutral pH, all synthesized CDs exhibited a negative zeta potential, between −10 to −22 mV, attributed to the presence of electronegative functional groups on their surface (**Figure 5**). This negative charge is essential for maintaining colloidal stability and interaction with the hydrogel, as it helps to prevent aggregation by providing electrostatic repulsion between individual particles.

Zeta potential analysis revealed that torrefaction pre-treatment significantly enhanced the magnitude of negative surface charge in CDs derived from almond peel (AP: −11±2 to −22±2 mV) and seeds (BS: -14±1 to -20±2 mV), while reducing it for bitter peel (BP: −22±2 to −16±2 mV). Two-way ANOVA confirmed a significant biomass-pre-treatment interaction ($p < 0.001$), demonstrating that pre-treatment directionally modulates zeta potential in a biomass-specific manner: intensifying negativity for AP and BS but attenuating it for BP. Biomass type alone showed no statistically significant effect ($p = 0.072$). This discrepancy suggests that the torrefaction process has varying effects on the surface chemistry of the different biomass sources, potentially due to the distinct composition and structure of the starting materials.[87] The enhanced negative charge in AP and

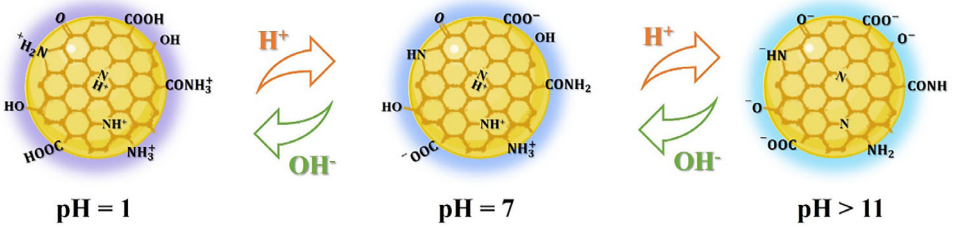

Figure 5. pH-dependent changes of CDs due to the protonation and deprotonation of the different functional surface groups.

BS CDs is indicative of an increase in carboxyl and hydroxyl functional groups as observed in FTIR spectra showing distinct peaks corresponding to the presence of functional groups such as —COOH and—OH.

The surface charge and functional group chemistry of CDs are strongly influenced by pH, which in turn modulates their fluorescence properties. Protonation and deprotonation of functional groups, particularly carboxyl (—COOH) and amino ($—NH_2$) moieties, alter the surface electronic environment and affect radiative transitions.[88,89] To investigate the pH sensitivity of CDs synthesized from both untreated and thermally pretreated biomass, UV–vis absorbance and fluorescence emission spectra were recorded over a wide pH range (1–13).

The PL intensity of CDs derived from AP and BS remained relatively stable between pH 3 and 11, with maximum emission observed at pH 7 and pH 5, respectively. In contrast, thermally pretreated samples (P-AP and P-BS) exhibited peak emission at lower pH values (pH 3 and 5, respectively), indicating that torrefaction alters surface states, shifting the optimal emission to more acidic environments (**Figure 6**a–c). For butternut peel-derived CDs (BP), the PL intensity showed a linear correlation with pH in the range of 3 to 11 ($R^2 = 0.997$), confirming their suitability as pH-responsive fluorescent probes. After pretreatment, P-BP exhibited maximum emission at pH 5, again reflecting surface state modification (Figure 6b).

All CD samples exhibited a marked decrease in PL intensity under strongly acidic (pH 1) and highly alkaline (pH 13) conditions. This quenching is attributed to protonation-induced aggregation or deprotonation-induced changes in the surface molecular structure, which disrupt electron-hole recombination pathways and result in weaker emission.[88] Across all samples, an increase in pH induced a minor bathochromic shift in the emission maximum, with pretreated CDs showing slightly more pronounced red shifts. These shifts suggest enhanced conjugation or oxygen-rich functionalization due to torrefaction, which may increase delocalization of π-electrons across the carbon core.

pH cycling experiments confirmed the reversibility of fluorescence emission for all samples (Figure S11, Supporting Information), highlighting their robustness under fluctuating environmental conditions. UV–vis absorption spectra further supported these observations. In untreated CDs, a $\pi \rightarrow \pi^*$ transition appeared as a shoulder ≈280 nm at pH 1 (marked i), which progressively blue-shifted to ≈265 nm as the pH increased (marked ii).[90] At higher pH levels, an $n \rightarrow \pi^*$ transition shoulder emerged ≈320 nm (marked iii), which became the dominant feature at pH ≥ 9 (marked iv).[91] After pretreatment, the UV–vis spectra became broader and less defined, likely due to increased surface heterogeneity and amorphous character (Figure S12, Supporting Information).

These results confirm that the pH-dependent PL behavior of the CDs is governed primarily by dynamic surface states modulated by the acid-base behavior of surface groups.[88] CDs prepared from pretreated biomass exhibited stronger emissions in acidic conditions, especially P-AP and P-BS, which are therefore suitable for deployment in low-pH environments such as acidified surface waters or industrial effluents. Surface state analysis (**Figure 5**) reveals that protonation-dependent charge modulation creates inherent selectivity: deprotonated carboxyl groups at pH > 5 selectively repel anions, while amino groups facilitate metal coordination. This could confer increased stability against common interferents: phenolic compounds are likely excluded through electrostatic repulsion at neutral pH, while transition metal-induced photoluminescence quenching may occur only under specific pH conditions.

Across the environmentally relevant pH range (5–9), all CD variants retained more than 85% of their fluorescence intensity, demonstrating strong optical stability in conditions representative of natural waters (e.g., rivers pH 6.5-8.5, lakes pH 6–9).[92] In addition to environmental robustness, the CDs exhibit inherent selectivity due to pH-tunable surface charge.[93] Pretreated P-AP and P-BS exhibit optimal emission at pH 3–5 and 5, respectively, suitable for acidic environments like acid rain-affected systems. At pH > 5, deprotonated carboxyl groups confer a net negative surface charge, resulting in electrostatic repulsion of negatively charged interferents such as phenolic compounds.[94] Simultaneously, amino groups may coordinate with metal ions, facilitating selective interactions depending on the ion's charge and coordination geometry.[93] This dual mechanism explains the observed fluorescence stability in the presence of common interferents and highlights the potential of these materials for selective pollutant detection in complex matrices.

4.3. Preparation and Characterization of CDs-Chitosan Hydrogels

CDs from pretreated almond peels, butternut peels, and seeds were then used to prepare a fluorescent chitosan hydrogel (**Figure 7**). The synthesized chitosan/CDs hydrogels exhibited distinct properties that were influenced by the concentration of CDs incorporated into the chitosan matrix. The incorporation process involved neutralization with 5N sodium hydroxide (NaOH), which facilitated the formation of hydrogels that were subsequently dried and cast into desired shapes. The control

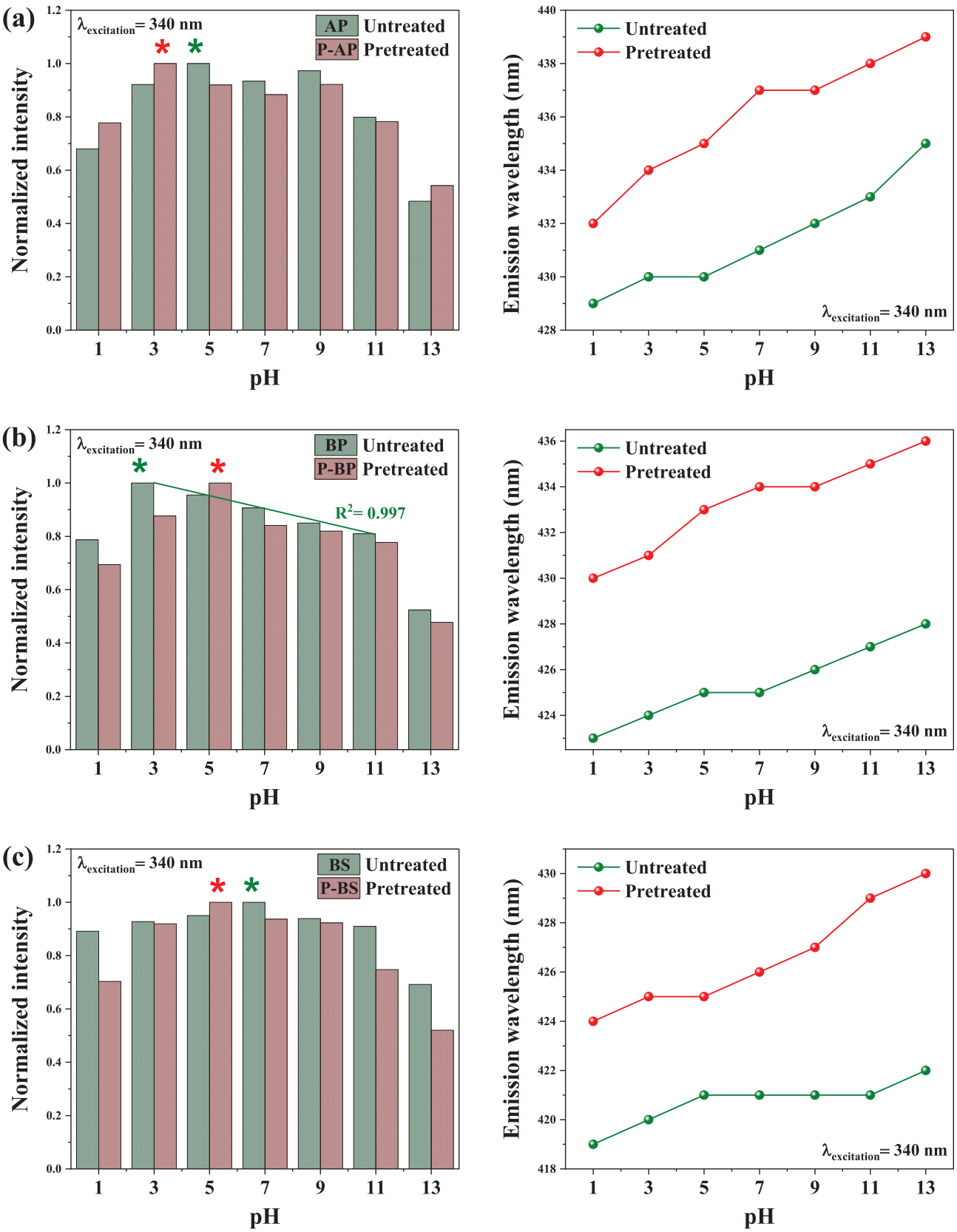

Figure 6. Effect of pH on fluorescence of CDs from pretreated and untreated almond peel a), butternut peels b), and seeds c). The lines correspond to the emission peak position, the histograms represent the normalized PL intensity, and the maxima are highlighted by an asterisk (*).

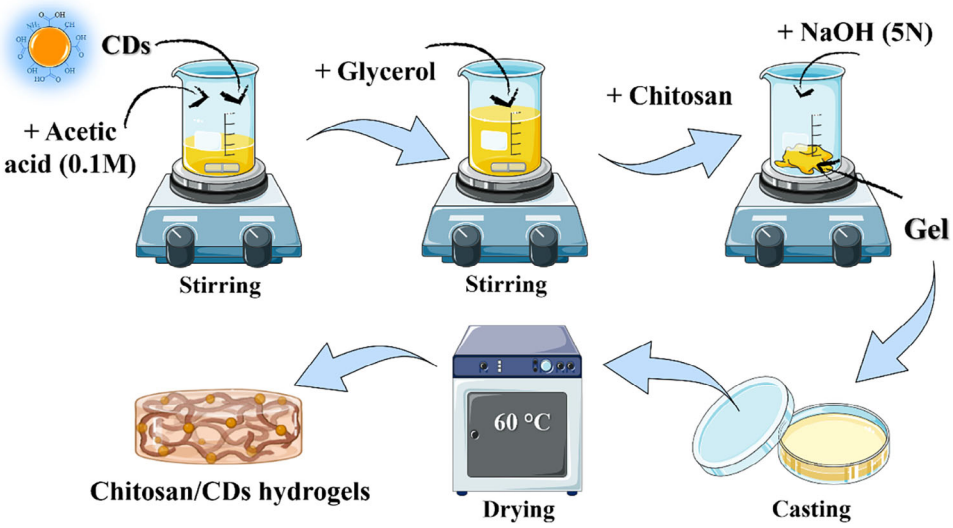

Figure 7. The preparation of chitosan/CDs hydrogels.

hydrogel (CH), which did not contain CDs, displayed a uniform and transparent appearance. In contrast, the introduction of CDs at varying concentrations (0.25, 0.5, and 1 wt.%) resulted in significant changes in both color and consistency, as evidenced by the samples labelled CH0.25, CH0.5, and CH1. As the concentration of CDs increased, the hydrogels transitioned to darker and more opaque forms, indicating successful integration of the CDs within the chitosan matrix. This change in appearance suggests that the interaction between the CDs and the chitosan network was enhanced with higher CD loading. Such interactions contribute to improving the potential functional fluorescence, which is characteristic of CDs due to their unique optical and electronic properties.[95,96]

FTIR spectra show similar peaks for chitosan and hydrogels, with variations in —OH, —NH, C—H, C—O—C, and C═O groups (Figure S12, Supporting Information). Hydrogen bonding (~3300 cm^{-1}) and C—H peaks (≈2900 cm^{-1}) are more pronounced in hydrogels, while ester bonds (1148 cm^{-1}) disappear, indicating reactions at primary amine groups. Hydrogels with CDs from different sources exhibit consistent functional group interactions.

Fluorescence data are presented in **Figure 8**. Fluorescence results show a consistent difference between hydrogels and pure P-BS-CDs. At 340 nm excitation wavelength, the photoluminescence (PL) emission of the hydrogel increases as the concentration of CDs increases, while the normal chitosan hydrogel without CDs does not exhibit any significant emission. This increase in PL intensity was accompanied by a gradual shift to shorter wavelengths.[97]

5. Detection of Pollutants

The fluorescence quenching behavior of chitosan hydrogels embedded with CDs derived from pretreated almond peels, butternut peels, and seeds was analyzed for the detection of MCPA and PCP as presented in Figures S13 and S14 (Supporting Information). All hydrogels demonstrated clear nonlinear quenching trends by increasing the quenchers concentration, well fitted to a logarithmic model $((F_0 - F)/F_0 = a.\ln[\text{Quencher}] + b$ with high R^2 values in the concentration of MPCA and PCP, ranging from 1 nM to 100 μM and from 5 nM to 50 μM, respectively

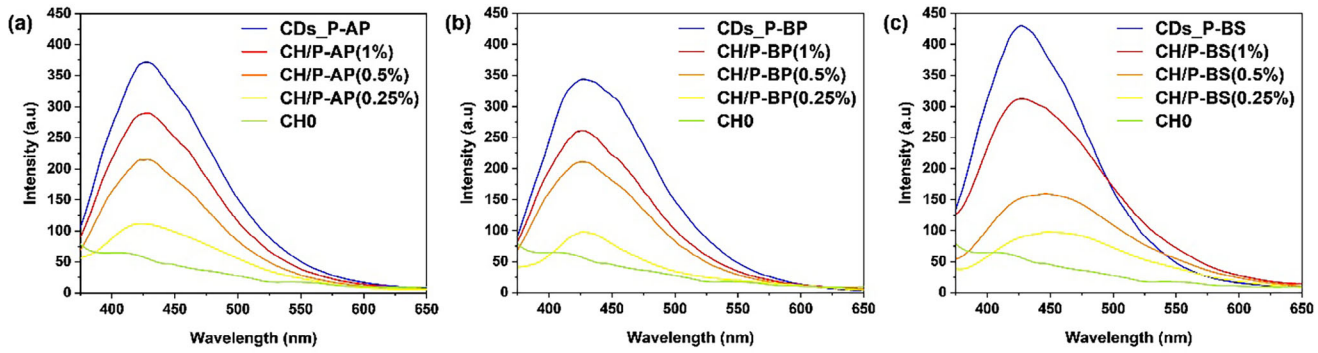

Figure 8. Fluorescence emission spectra of chitosan hydrogels with different loads (0%, 0.25%, 0.5%, 1%) of pretreated-butternut seeds carbon dots, in comparison to pure P-BS-CDs solution (0.5 mg mL^{-1}) at 340 nm excitation wavelength.

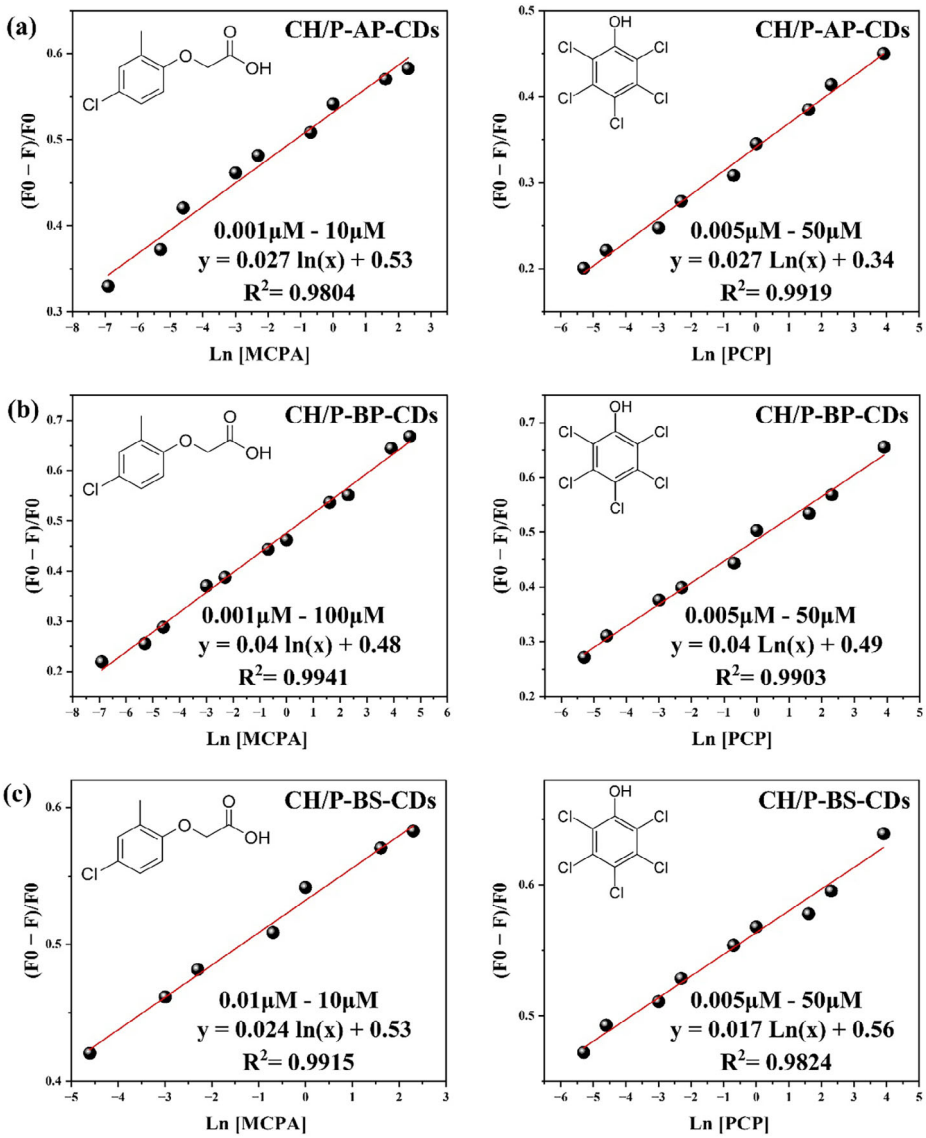

Figure 9. Quenching plots of chitosan hydrogels with 1% CDs derived from almond peels a), butternut peels b), and seeds c), under increasing MCPA and PCP concentrations (0–100 µM) (excitation wavelength 340 nm).

(**Figure 9**). This indicates a strong correlation between the experimental data and the fitted model. Among the hydrogels, CH/P-BP-CDs exhibited the highest sensitivity to both MCPA and PCP, as evidenced by the steepest slope (*a*) in the logarithmic fit, reflecting a higher quenching efficiency. CH/P-AP-CDs and CH/P-BS-CDs displayed slightly lower sensitivity, with CH/P-BS-CDs having the least pronounced response, particularly for PCP. These differences could be attributed to variations in the structural and chemical properties of the CDs derived from different precursors, such as their functional groups and aromaticity, which affect interactions with the quenchers through mechanisms like π-π stacking and hydrogen bonding.[98]

Such nonlinear quenching behavior is consistent with studies highlighting the role of static and dynamic quenching mechanisms in fluorescence systems involving aromatic and chlorinated quenchers.[99–101]

Table 1 summarizes the LOD and LOQ for MCPA and PCP, obtained using three different hydrogels: CH/P-AP-CDs, CH/P-BP-CDs, and CH/P-BS-CDs. Among these, the CH/P-BP-CDs hydrogel demonstrated the highest sensitivity, achieving the lowest

Table 1. LOD and LOQ of MCPA and PCP (100 nM) by different chitosan/CDs hydrogels.

Hydrogels	MCPA		PCP	
	LOD [nM]	LOQ [nM]	LOD [nM]	LOQ [nM]
CH/P-AP-CDs	4.18 ± 0.08	13.95 ± 0.26	1.51 ± 0.18	5.05 ± 0.60
CH/P-BP-CDs	4.10 ± 0.10	13.67 ± 0.34	1.45 ± 0.08	4.85 ± 0.28
CH/P-BS-CDs	4.23 ± 0.03	14.11 ± 0.09	1.67 ± 0.24	5.58 ± 0.80

Table 2. Comparison with previous works.

Pollutant	Material	Detection range	LOD	Refs.
PCP	Gold nanoclusters/graphene hybrids	0.01 pM – 0.1 nM	0.01 pM	[9]
	ZnO-nanocrystal-decorated N-doped graphene composites	0.5 pM – 61.1 nM	0.16 pM	[104]
	Silica xerogel thin film	10 nM – 1 μM	10 nm	[102]
	Biomass-derived CDs-Chitosan hydrogel	1 nM – 50 μM	1.45 nM	This work
MCPA	β-cyclodextrin carbon nanotube sensor	10 μM – 100 μM	0.99 μM	[105]
	PANI-β-CD/fMWCNT/GC film	10 μM – 50 μM	1.1 μM	[106]
	MoS_2-graphene quantum dots hybrid nanocomposite	10 pM – 0.1 μM	5.5 pM	[91]
	Biomass-derived CDs-Chitosan hydrogel	10 nM – 10 μM	4.10 nM	This work

LOD values for MCPA (4.10 ± 0.10 nM) and PCP (1.45 ± 0.08 nM). Similarly, the CH/P-BP-CDs hydrogel exhibited the lowest LOQ values for both analytes, underpinning its superior sensitivity. This system outperformed other reported sensors, being 10 times more sensitive than silica xerogel thin film for PCP detection[102] and 2.44 times more sensitive than β-cyclodextrin carbon nanotube sensors for MCPA detection.[103]

Comparative analysis (**Table 2**) confirms the competitive sensitivity of our sustainable CD-chitosan hydrogel sensor. While some engineered nanomaterials achieve lower absolute detection limits for PCP (e.g., 0.01 pM using Au nanoclusters/graphene).[9] or MCPA (5.5 pM using MoS_2-GQDs),[90] our system delivers practically relevant sub-nanomolar LODs (1.45 nM for PCP; 4.10 nM for MCPA) that significantly surpass key regulatory thresholds (EU: 0.5 μg L^{-1} PCP ≈ 1.88 nM; WHO: 2 μg L^{-1} MCPA ≈ 9.3 nM). Crucially, our sensor integrates three distinct advantages over prior art: sustainable sourcing from food waste (vs synthetic precursors/metals); operational robustness via a reusable hydrogel matrix (vs fragile films or complex hybrids); and exceptional advancement for MCPA detection, outperforming prior carbon-based sensors[104,105] by >200-fold in sensitivity. This balance of performance, practicality, and eco-design underscores its viability for real-world pollutant monitoring.

The chitosan hydrogel containing 1% of carbon dots derived from pretreated almond peels, butternut peels and seeds constituted a luminescence "turn-off" sensor for the chlorinated phenols in aqueous media. Recycling experiments (Figure S15, Supporting Information) revealed a gradual decrease in fluorescence intensity over five regeneration and reuse cycles, with the reduction being more pronounced for PCP compared to MCPA. After exposure to 100 μM of PCP and MCPA, the detection efficiency decreased by ≈10%, reaching ≈90% of the initial value for all hydrogels. These results indicate good structural integrity and photostability over repeated cycles. Among the tested materials, CH/P-BP-CDs exhibited the best overall performance, showing slower fluorescence quenching compared to CH/P-AP-CDs and CH/P-BS-CDs. In contrast, CH/P-BS-CDs were the most affected by quenching.

6. Conclusion and Perspectives

In conclusion, this study demonstrates the use of biomass-CDs integrated into chitosan hydrogels for the sensitive detection of toxic aromatic pollutants. The microwave synthesis of CDs from kitchen waste materials, such as almond peels and butternut peels, and seeds, highlights an eco-friendly and sustainable method for converting discarded provisions into valuable functional resources. Notably, this work provides a systematic investigation into the effect of biomass pretreatment on the optical properties of the resulting CDs, a previously unstudied aspect. The unique fluorescence properties of these CDs, which are influenced by their size, their pH sensitivity, and excitation wavelength, reveal a significant advancement in the field of sensor technology. The enhancement of fluorescence intensity through thermal pretreatment further emphasizes the importance of optimizing synthesis conditions and the precursor conditioning to achieve superior detection capabilities.

The application of these CDs to develop fluorescent chitosan hydrogels for detecting PCP and MCPA highlights their practical potential in environmental remediation. The system achieved high sensitivity, with detection limits of 4.10 ± 0.10 nM for MCPA and 1.45 ± 0.08 nM for PCP, enabling the detection of hazardous substances at low concentrations in diverse environmental matrices. Integrating sustainable materials enhances sensor performance while exemplifying a circular economy approach, converting waste into valuable resources for advanced environmental monitoring, and aligns with the principles of green chemistry and sustainable scientific practices. While these highlights promise for environmental monitoring, future work will address:

- Fundamental mechanisms via fluorescence lifetime measurements and molecular docking simulations,
- Deployment readiness through long-term stability assessments (>6 months) and interference (common phenolic compounds and metal ions) validation,
- Verification in environmental water samples (river water, lake water);
- Scalability of production and pretreatment optimization for broader applications. This approach exemplifies circular economy principles, converting waste into advanced sensing platforms while adhering to green chemistry tenets.

Supporting Information

Supporting Information is available from the Wiley Online Library or from the author.

Acknowledgements

The authors would like to acknowledge the financial support from the Quebec Centre for Advanced Materials (CQMF/QCAM) from Fonds de recherche du Québec–Nature et Technologies (FRQNT). F.R. acknowledges NSERC for an individual Discovery Grant (RGPIN-2023-05357). COP acknowledges a contribution from the Canada Research Chair program (CRC-2019-00074). D.B. acknowledges FRQNT Postdoctoral Fellowship (No. 316170) for the financial support.

Conflict of Interest

The authors declare no conflict of interest.

Data Availability Statement

The data that support the findings of this study are available from the corresponding author upon reasonable request.

Keywords

carbon dots, chlorophenols, fluorescent hydrogels, kitchen waste, microwave synthesis, thermal pretreatment

Received: May 28, 2025
Revised: July 16, 2025
Published online:

[1] A. Zada, M. Khan, M. A. Khan, Q. Khan, A. Habibi-Yangjeh, A. Dang, M. Maqbool, *Environ. Res.* **2021**, *195*, 110742.
[2] K. Kumari, R. Jain, in *Pollutants of Global Concern: A Comprehensive Overview of Persistent Organic Pollutants* (Ed.: K. Kumari), Springer, Cham, **2024**, 261–284, ISBN 978-3-031-50996-4.
[3] A. Cabrera, L. Cox, K. A. Spokas, R. Celis, M. C. Hermosín, J. Cornejo, W. C. Koskinen, *J. Agric. Food Chem.* **2011**, *59*, 12550.
[4] WHO, *Guidelines for Drinking-Water Quality, 4th ed.*, WHO Press, Switzerland **2011**, ISBN 978-92-4-154761-1.
[5] P. A. Morton, C. Fennell, R. Cassidy, D. Doody, O. Fenton, P. E. Mellander, P. Jordan, *Wiley Interdiscip. Rev. Water* **2020**, *7*, 1402.
[6] W. Wu, H. Xiao, S. Luo, C. Liu, Y. Tang, L. Yang, *Sens. Actuators, B* **2016**, *222*, 747.
[7] N. Fattahi, Y. Assadi, M. R. M. Hosseini, E. Z. Jahromi, *J. Chromatogr. A* **2007**, *1157*, 23.
[8] W. Liu, J. Zha, X. Meng, J. Wu, C. Sun, P. Qiu, M. Fizir, H. He, *Anal. Methods* **2017**, *9*, 4581.
[9] S. Luo, H. Xiao, S. Yang, C. Liu, J. Liang, Y. Tang, *Sens. Actuators, B* **2014**, *194*, 325.
[10] Y. Ye, C. Huang, J. Yang, Y. Li, Q. Zhuang, J. Gu, *Microporous Mesoporous Mater.* **2019**, *284*, 36.
[11] Q. Zhang, X. Wang, L. Yuan, L. Yu, C. Shao, H. Jia, S. Lu, *Anal. Methods* **2024**, *16*, 2063.
[12] J. Chen, X. Xia, P. Li, H. Yu, Y. Xie, Y. Guo, W. Yao, H. Qian, Y. Cheng, *Food Chem.* **2023**, *405*, 134802.
[13] S. Ansari, S. Masoum, *Talanta* **2021**, *223*, 121411.
[14] Y. Li, D. J. Young, X. J. Loh, *Mater. Chem. Front.* **2019**, *3*, 1489.
[15] X. Pan, Q. Wang, D. Benetti, Y. Ni, F. Rosei, *Nano Energy* **2022**, *103*, 107718.
[16] P. K. Marvi, P. Das, A. Jafari, S. Hassan, H. Savoji, S. Srinivasan, A. R. Rajabzadeh, *Adv. Healthcare Mater.* **2025**, *14*, 2403876.
[17] D. Buenger, F. Topuz, J. Groll, *Prog. Polym. Sci.* **2012**, *37*, 1678.
[18] M. C. Catoira, L. Fusaro, D. Di Francesco, M. Ramella, F. Boccafoschi, *J. Mater. Sci.: Mater. Med.* **2019**, *30*, 115.
[19] N. Bhattarai, J. Gunn, M. Zhang, *Adv. Drug Delivery Rev.* **2010**, *62*, 83.
[20] I. Haddadou, A. Ami, J. Gagnon, C. M. Ouellet-Plamondon, *Mater. Today Chem.* **2025**, *46*, 102719.
[21] A. T. Nkeumaleu, D. Benetti, I. Haddadou, M. Di Mare, C. M. Ouellet-Plamondon, F. Rosei, *RSC Adv.* **2022**, *12*, 11621.
[22] J. Guo, W. Lu, H. Zhang, Y. Meng, F. Du, S. Shuang, C. Dong, *Sens. Actuators, B* **2021**, *330*, 129360.
[23] Z. Cheng, S. Wu, *Adv. Sustainable Syst.* **2025**, *9*, 2400663.
[24] C. Ji, Y. Zhou, R. M. Leblanc, Z. Peng, *ACS Sens.* **2020**, *5*, 2724.
[25] A. Kumar, S. Asu, P. Mukherjee, P. Singh, A. Kumari, S. K. Sahu, *J. Photochem. Photobiol., A Chem.* **2021**, *406*, 113019.
[26] H. Li, X. Yan, D. Kong, R. Jin, C. Sun, D. Du, Y. Lin, G. Lu, *Nanoscale Horiz.* **2020**, *5*, 218.
[27] C. Liu, W. Fan, W. X. Cheng, Y. Gu, Y. Chen, W. Zhou, X. F. Yu, M. Chen, M. Zhu, K. Fan, *Adv. Funct. Mater.* **2023**, *33*, 2370116.
[28] S. D. Hettiarachchi, R. M. Graham, K. J. Mintz, Y. Zhou, S. Vanni, Z. Peng, R. M. Leblanc, *Nanoscale* **2019**, *11*, 6192.
[29] W. Zhang, N. Kandel, Y. Zhou, N. Smith, B. C. Ferreira, M. Perez, M. L. Claure, K. J. Mintz, C. Wang, R. M. Leblanc, *J. Colloid Interface Sci.* **2022**, *623*, 617.
[30] Y.-F. Wu, H.-C. Wu, C.-H. Kuan, C.-J. Lin, L.-W. Wang, C.-W. Chang, T.-W. Wang, *Sci. Rep.* **2016**, *6*, 21170.
[31] D. Benetti, E. Jokar, C.-H. Yu, A. Fathi, H. Zhao, A. Vomiero, E. W.-G. Diau, F. Rosei, *Nano Energy* **2019**, *62*, 781.
[32] D. Benetti, F. Rosei, *Nanoenergy Adv.* **2022**, *2*, 222.
[33] T. Mandal, S. R. Mishra, M. Kumar, V. Singh, *Sustainable Energy Fuels* **2024**, *8*, 5638.
[34] Y.-P. Sun, *Carbon dots: Exploring Carbon at Zero-Dimension*, Springer Nature, London **2020**.
[35] M. L. Liu, B. B. Chen, C. M. Li, C. Z. Huang, *Green Chem.* **2019**, *21*, 449.
[36] J. Schneider, C. J. Reckmeier, Y. Xiong, M. von Seckendorff, A. S. Susha, P. Kasák, A. L. Rogach, *J. Phys. Chem. C* **2017**, *121*, 2014.
[37] P. Das, S. Ganguly, M. Bose, S. Mondal, A. K. Das, S. Banerjee, N. C. Das, *Mater. Sci. Eng., C* **2017**, *75*, 1456.
[38] Z. Ramezani, M. Qorbanpour, N. Rahbar, *Colloids Surf. A* **2018**, *549*, 58.
[39] Y. Ma, M. Zhang, H. Wang, B. Wang, H. Huang, Y. Liu, Z. Kang, *Mater. Today Commun.* **2020**, *24*, 101222.
[40] J. George, M. Balachandran, *Adv. Sustainable Syst.* **2025**, *9*, 2400938.
[41] M. Xue, M. Zou, J. Zhao, Z. Zhan, S. Zhao, *J. Mater. Chem. B* **2015**, *3*, 6783.
[42] S. Pandiyan, L. Arumugam, S. P. Srirengan, R. Pitchan, P. Sevugan, K. Kannan, G. Pitchan, T. A. Hegde, V. Gandhirajan, *ACS Omega* **2020**, *5*, 30363.
[43] W. L. Ang, C. A. L. Boon Mee, N. S. Sambudi, A. W. Mohammad, C. P. Leo, E. Mahmoudi, M. Ba-Abbad, A. Benamor, *Sci Rep.* **2020**, *10*, 21199.
[44] U. Gul, S. Kanwal, S. Tabassum, M. A. Gilani, A. Rahim, *Microchim. Acta* **2020**, *187*, 135.
[45] M. J. C. van der Stelt, H. Gerhauser, J. H. A. Kiel, K. J. Ptasinski, *Biomass Bioenergy* **2011**, *35*, 3748.
[46] J. Wu, T. Chen, S. Ge, W. Fan, H. Wang, Z. Zhang, E. Lichtfouse, T. Van Tran, R. K. Liew, M. Rezakazemi, R. Huang, *Environ. Chem. Lett.* **2023**, *21*, 3393.
[47] M. Joshi, S. Manjare, *Environ. Sci. Pollut. Res.* **2024**, *31*, 48928.
[48] J. Xu, L. Zhu, W. Cai, Z. Ding, D. Chen, W. Zhang, C. Xing, K. Wang, Z. Ma, *Chem. Eng. J.* **2024**, *494*, 153044.
[49] T. V. de Medeiros, J. Manioudakis, F. Noun, J.-R. Macairan, F. Victoria, R. Naccache, *J. Mater. Chem. C* **2019**, *7*, 7175.
[50] S. Sahana, A. Gautam, R. Singh, S. Chandel, *Nat. Prod. Bioprospect.* **2023**, *13*, 51.

[51] H. Dang, L.-K. Huang, Y. Zhang, C.-F. Wang, S. Chen, *Ind. Eng. Chem. Res.* **2016**, *55*, 5335.
[52] N. Brun, S.-H. Yu, R. J. White, *Porous Carbon Materials from Sustainable Precursors*, Royal Society of Chemistry, London, UK **2015**.
[53] I. K. M. Yu, H. Chen, F. Abeln, H. Auta, J. Fan, V. L. Budarin, J. H. Clark, S. Parsons, C. J. Chuck, S. Zhang, G. Luo, D. C. W. Tsang, *Crit. Rev. Environ. Sci. Technol.* **2021**, *51*, 1479.
[54] R. B. González-González, L. T. González, M. Madou, C. Leyva-Porras, S. O. Martinez-Chapa, A. Mendoza, *Nanomaterials* **2022**, *12*, 298.
[55] M. Otten, M. Hildebrandt, R. Kühnemuth, M. Karg, *Langmuir* **2022**, *38*, 6148.
[56] Y. Zhao, S. Jing, X. Peng, Z. Chen, Y. Hu, H. Zhuo, R. Sun, L. Zhong, *Cellulose* **2020**, *27*, 415.
[57] G. Liu, B. Li, Y. Liu, Y. Feng, D. Jia, Y. Zhou, *Appl. Surf. Sci.* **2019**, *487*, 1167.
[58] Y. Yang, J. Cui, M. Zheng, C. Hu, S. Tan, Y. Xiao, Q. Yang, Y. Liu, *Chem. Commun.* **2012**, *48*, 380.
[59] S. Jing, Y. Zhao, R.-C. Sun, L. Zhong, X. Peng, *ACS Sustainable Chem. Eng.* **2019**, *7*, 7833.
[60] F. Xu, J. Yu, T. Tesso, F. Dowell, D. Wang, *Appl. Energy* **2013**, *104*, 801.
[61] D. Özçimen, A. Ersoy-Meriçboyu, *Renew. energy* **2010**, *35*, 1319.
[62] A. Zheng, L. Jiang, Z. Zhao, Z. Huang, K. Zhao, G. Wei, X. Wang, F. He, H. Li, *Energy Fuels* **2015**, *29*, 8027.
[63] A. Dager, T. Uchida, T. Maekawa, M. Tachibana, *Sci. Rep.* **2019**, *9*, 14004.
[64] V. Ţucureanu, A. Matei, A. M. Avram, *Crit. Rev. Anal. Chem.* **2016**, *46*, 502.
[65] M. C. Ortega-Liebana, J. L. Hueso, S. Ferdousi, R. Arenal, S. Irusta, K. L. Yeung, J. Santamaria, *Appl. Catal., B* **2017**, *218*, 68.
[66] J. Hou, H. Li, L. Wang, P. Zhang, T. Zhou, H. Ding, L. Ding, *Talanta* **2016**, *146*, 34.
[67] T. Ogi, H. Iwasaki, K. Aishima, F. Iskandar, W.-N. Wang, K. Takimiya, K. Okuyama, *RSC Adv.* **2014**, *4*, 55709.
[68] X. Lin, M. Xiong, J. Zhang, C. He, X. Ma, H. Zhang, Y. Kuang, M. Yang, Q. Huang, *Microchem. J.* **2021**, *160*, 105604.
[69] L. Zhai, X.-M. Ren, Q. Xu, *Mater. Chem. Front.* **2021**, *5*, 4272.
[70] L. Li, T. Dong, *J. Mater. Chem. C* **2018**, *6*, 7944.
[71] K. Anpalagan, H. Yin, I. Cole, T. Zhang, D. T. H. Lai, *Inorganics* **2024**, *12*, 96.
[72] I. Kaur, V. Batra, N. K. R. Bogireddy, J. Baveja, Y. Kumar, V. Agarwal, *iScience* **2024**, *27*, 108920.
[73] G. Kalaiyarasan, J. Joseph, P. Kumar, *ACS Omega* **2020**, *5*, 22278.
[74] H. Li, J. Zheng, Y. Yang, L. Chen, X. Liu, *Adv. Opt. Mater.* **2025**, *13*, 2500148.
[75] Q. Xu, B. Li, Y. Ye, W. Cai, W. Li, C. Yang, Y. Chen, M. Xu, N. Li, X. Zheng, *Nano Res.* **2018**, *11*, 3691.
[76] A. Sangjan, S. Boonsith, K. Sansanaphongpricha, T. Thinbanmai, S. Ratchahat, N. Laosiripojana, K. C.-W. Wu, H. S. Shin, C. Sakdaronnarong, *Sci. Rep.* **2022**, *12*, 10550.
[77] M. Xu, Q. Huang, R. Sun, X. Wang, *RSC Adv.* **2016**, *6*, 88674.
[78] P. M. Gharat, J. M. Chethodil, A. P. Srivastava, P. Praseetha, H. Pal, S. D. Choudhury, *Photochem. Photobiol. Sci.* **2019**, *18*, 110.
[79] W. Liu, C. Li, X. Sun, W. Pan, G. Yu, J. Wang, *Nanotechnology* **2017**, *28*, 485705.
[80] Y. Feng, D. Zhong, H. Miao, X. Yang, *Talanta* **2015**, *140*, 128.
[81] A.-M. Alam, B.-Y. Park, Z. K. Ghouri, M. Park, H.-Y. Kim, *Green Chem.* **2015**, *17*, 3791.
[82] A. Sachdev, P. Gopinath, *Analyst* **2015**, *140*, 4260.
[83] N. Tejwan, S. K. Saha, J. Das, *Adv. Colloid Interface Sci.* **2020**, *275*, 102046.
[84] M. Chen, C. Liu, H. Sun, F. Yang, D. Hou, Y. Zheng, R. Shi, X. He, X. Lin, *ACS Appl. Mater. Interfaces* **2024**, *16*, 9182.
[85] A. Prasannan, T. Imae, *Ind. Eng. Chem. Res.* **2013**, *52*, 15673.
[86] T. C. Wareing, P. Gentile, A. N. Phan, *ACS Nano* **2021**, *15*, 15471.
[87] L. Zhu, D. Shen, C. Wu, S. Gu, *Ind. Eng. Chem. Res.* **2020**, *59*, 22017.
[88] D. Bharathi, B. Siddlingeshwar, R. H. Krishna, V. Singh, N. Kottam, D. D. Divakar, A. A. Alkheraif, *J. Fluoresc.* **2018**, *28*, 573.
[89] L. Yuan, C. Shao, Q. Zhang, E. Webb, X. Zhao, S. Lu, *Environ. Res.* **2024**, *251*, 118610.
[90] V. Sharma, P. Tiwari, S. M. Mobin, *J. Mater. Chem. B* **2017**, *5*, 8904.
[91] Y. Yang, G. Fang, X. Wang, F. Zhang, J. Liu, W. Zheng, S. Wang, *Electrochim. Acta* **2017**, *228*, 107.
[92] Warner, S. SDG Indicator 6.3.2 Technical Guidance Document NO.2: Target Values (UNEP GEMS/Water, **2020**).
[93] H. Ehtesabi, Z. Hallaji, S. Najafi Nobar, Z. Bagheri, *Microchim. Acta* **2020**, *150*, 187.
[94] W. K. Szapoczka, A. L. Truskewycz, T. Skodvin, B. Holst, P. J. Thomas, *Sci. Rep.* **2023**, *13*, 10660.
[95] Y. J. Chung, J. Kim, C. B. Park, *ACS Nano* **2020**, *14*, 6470.
[96] K. K. Kłosiński, R. A. Wach, M. K. Girek-Bąk, B. Rokita, D. Kołat, Ż. Kałuzińska-Kołat, B. Kłosińska, Ł. Duda, Z. W. Pasieka, *Polymers* **2022**, *15*, 144.
[97] Y. Ma, X. Zhang, J. Bai, K. Huang, L. Ren, *Chem. Eng. J.* **2019**, *374*, 787.
[98] F. Zu, F. Yan, Z. Bai, J. Xu, Y. Wang, Y. Huang, X. Zhou, *Microchim. Acta* **2017**, *184*, 1899.
[99] S. Yang, J. Liang, S. Luo, C. Liu, Y. Tang, *Anal. Chem.* **2013**, *85*, 7720.
[100] S. Li, L. Nie, W. Wen, Z. Wang, J. Wang, S. Wang, *Food Bioengineering* **2022**, *1*, 212.
[101] P. M. Gharat, H. Pal, S. D Choudhury, *Spectrochim. Acta, Part A* **2019**, *209*, 14.
[102] C. Tang, G. Meng, Q. Huang, Z. Huang, X. Zhang, M. Wang, *Sens. Actuators, B* **2012**, *332*, 171.
[103] C. Zanoni, S. Spina, L. R. Magnaghi, M. Guembe-Garcia, R. Biesuz, G. Alberti, *Int. J. Environ. Res. Public Health* **2022**, *19*, 16488.
[104] D. Jiang, X. Du, Q. Liu, L. Zhou, J. Qian, K. Wang, *ACS Appl. Mater. Interfaces* **2015**, *7*, 3093.
[105] V. Rahemi, J. Vandamme, J. Garrido, F. Borges, C. Brett, E. Garrido, *Talanta* **2012**, *99*, 288.
[106] V. Rahemi, J. Garrido, F. Borges, C. Brett, E. Garrido, *Environ. Sci. Pollut. Res.* **2015**, *22*, 4491.